2011 50th IEEE Conference on Decision and Control and
European Control Conference (CDC-ECC)
Orlando, FL, USA, December 12-15, 2011

A Numerical Study on Controlling a Nonlinear Multilink Arm Using A Retrospective Cost Model Reference Adaptive Controller

Matthew W. Isaacs*, Jesse B. Hoagg†, Alexey V. Morozov‡, and Dennis S. Bernstein§

***Abstract*— We address the model reference adaptive control problem for a nonlinear multilink planar arm mechanism, where links are interconnected by torsional springs and dashpots, a control torque is applied to the hub of the mechanism, and the objective is to control the angular position of the last link. It is known that the linearized transfer function for the multilink planar arm has nonminimum-phase zeros when the control torque and angular position sensor are not colocated. We use a retrospective cost model reference adaptive control (RC-MRAC) algorithm, which is effective for nonminimum-phase systems provided that the nonminimum-phase zeros are known. We demonstrate that RC-MRAC effectively controls the multilink arm for a range of reference model command signal amplitudes and frequencies.**

I. Introduction

The multilink planar arm mechanism consists of N links, which are interconnected by torsional springs and dashpots. This mechanism is an approximation of a flexible rotating arm or bending beam, whose dynamics and control are studied for applications such as space structures [1], [2] and hard drives [3], [4]. The multilink planar arm presents a challenging control problem because the system is nonlinear and exhibits nonminimum-phase behavior, as shown in [5, Chap. 8.5] for the 2-link case and [6] for the N-link case.

Nonmimum-phase zeros can create challenges for feedback control systems by limiting bandwidth and gain margins [7], and causing initial undershoot or direction reversals in the step response [8], [9]. Thus, it is of interest to determine physical properties in mechanical systems that give rise to nonminimum-phase zeros. The colocated force-to-velocity transfer functions for flexible structures are known to be positive real (and thus minimum phase) [10]. This property suggests that sensor-actuator noncolocation may cause nonminimum-phase zeros; however, [11], [12] demonstrate that noncolocation alone is not the source of nonminimum-phase zeros. In particular, [11] considers a string of masses interconnected by linear springs and dashpots, and shows that the noncolocated transfer functions from the force on one mass to the position of another mass are minimum phase.

The bending-beam examples considered in [13], [14] suggest that nonminimum-phase zeros may arise from sensor-actuator noncolocation combined with rotational motion. This conjecture is supported by the results of [6], which shows that the noncolocated transfer functions of the linearized multilink planar arm have nonminimum-phase zeros.

While nonminimum-phase zeros can be challenging for many control methodologies, they are particularly challenging for adaptive controllers. For discrete-time systems with nonminimum-phase zeros, retrospective cost adaptive control (RCAC) techniques are known to be effective provided that the nonminimum-phase zeros are known [15]–[17]. In [6], RCAC is used to control the 2-link planar arm mechanism using knowledge of only the first non-zero Markov parameter and the nonmimum-phase zeros of the discretized linearized transfer function from hub torque to angular position.

In the present paper, we extend the work of [6] in two ways. First, we adopt the retrospective cost model reference adaptive control (RC-MRAC) algorithm, which is presented in [18]. The simulation results of this paper demonstrate that RC-MRAC effectively controls the multilink arm for a wide range of reference model command signal amplitudes and frequencies. The second extension presented in this paper is the adaptive control of the multilink arm with more than 2 links. Specifically, we address the 2-link, 3-link, and 4-link cases.

II. Equations of Motion

In this section, we review the nonlinear equations of motion for an N-link planar arm, and present the linearized equations of motion. For a detailed derivation, see [6].

First, let p_1 be the point where the first link is connected to the horizontal plane, and, for $i = 2, ..., N$, let p_i be the point where the i^{th} link is connected to the $(i-1)^{\text{th}}$ link. Next, for $i = 1, ..., N$, let m_i be the mass of the i^{th} link, let l_i be the length of the i^{th} link, let c_i be the damping at the joint p_i, let k_i be the stiffness of the joint p_i, and let $I_i \triangleq \frac{1}{12} m_i l_i^2$ be the moment of inertia of the i^{th} link about its center of mass.

Next, we define the inertial frame F_A with orthogonal unit vectors $(\hat{\imath}_{\mathrm{A}}, \hat{\jmath}_{\mathrm{A}}, \hat{k}_{\mathrm{A}})$, where $\hat{\imath}_{\mathrm{A}}$ and $\hat{\jmath}_{\mathrm{A}}$ lie in the plane of motion of the N-link planar arm, and $\hat{k}_{\mathrm{A}}$ is orthogonal to the plane of motion. For simplicity, we assume that the origin of F_{A} is located at p_1. Finally, for $i = 1, \ldots, N$, let θ_i be the angle from $\hat{\imath}_{\mathrm{A}}$ to the vector from p_i to p_{i+1}. The N-link planar arm is shown in Figure 1.

A. Nonlinear Equations of Motion

For $i = 1, \ldots, N$, the kinetic energy of the i^{th} link is $T_i \triangleq \frac{1}{2} m_i V_i^2 + \frac{1}{2} I_i \dot{\theta}_i^2$, where the magnitude of the translational velocity of the i^{th} link is given by

*Graduate Student, Department of Mechanical Engineering, The University of Kentucky, Lexington, KY, 40506-0503, email: matthew.isaacs@uky.edu.

†Assistant Professor, Department of Mechanical Engineering, The University of Kentucky, Lexington, KY, 40506-0503, email: jhoagg@engr.uky.edu.

‡Graduate Student, Department of Aerospace Engineering, University of Michigan, Ann Arbor, MI 48109, email: morozova@umich.edu.

§Professor, Department of Aerospace Engineering, University of Michigan, Ann Arbor, MI 48109, email: dsbaero@umich.edu.

978-1-61284-799-3/11/$26.00 ©2011 IEEE

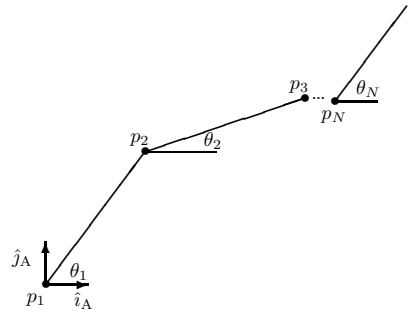

Fig. 1. All motion of the N-link planar arm is in the horizontal plane.

$$V_i = \left[\tfrac{1}{4} l_i^2 \dot{\theta}_i^2 + \sum_{j=1}^{i-1} \left(l_j^2 \dot{\theta}_j^2 + l_i l_j \dot{\theta}_i \dot{\theta}_j \cos(\theta_j - \theta_i) \right) + 2 \sum_{j \neq h}^{i-1} l_j l_h \dot{\theta}_j \dot{\theta}_h \cos(\theta_j - \theta_h) \right]^{1/2}.$$

The total kinetic energy is defined by $T \triangleq \sum_{i=1}^{N} T_i$. Next, for $i = 1, \ldots, N$, the potential energy of the i^{th} link is

$$U_i \triangleq \begin{cases} \frac{1}{2} k_1 \theta_1^2, & i = 1, \\ \frac{1}{2} k_i (\theta_{i-1} - \theta_i)^2, & i > 1, \end{cases}$$

and the total potential energy is defined by $U \triangleq \sum_{i=1}^{N} U_i$. Thus, the Lagrangian for the N-link system is $L \triangleq T - U$.

Next, for $i = 1, \ldots, N$, let F_{c_i} be the dissipation function resulting from the damping at joint p_i, that is,

$$F_{c_i} \triangleq \begin{cases} \frac{1}{2} c_1 \dot{\theta}_1^2, & i = 1, \\ \frac{1}{2} c_i (\dot{\theta}_{i-1} - \dot{\theta}_i)^2, & i > 1, \end{cases}$$

and define $F_c \triangleq \sum_{i=1}^{N} F_{c_i}$. For $i = 1, \ldots, N$, let v_i be an external torque applied at p_i. Thus, for $i = 1, \ldots, N$ the nonlinear equations of motion are given by

$$\frac{d}{dt} \frac{\partial L}{\partial \dot{\theta}_i} - \frac{\partial L}{\partial \theta_i} + \frac{\partial F_c}{\partial \dot{\theta}_i} = v_i. \tag{1}$$

B. Linearized Equations of Motion

Now, we present the linearized equations of motion for the N-link system. First, define $\Theta \triangleq \begin{bmatrix} \theta_1 & \ldots & \theta_N \end{bmatrix}^{\mathrm{T}}$, and $\Upsilon \triangleq \begin{bmatrix} v_1 & \ldots & v_N \end{bmatrix}^{\mathrm{T}}$. We linearize about the $(\Theta, \dot{\Theta}) \equiv 0$ equilibrium. Let $\delta\Theta$ be the linear approximation of Θ around the equilibrium $(\Theta, \dot{\Theta}) \equiv 0$.

Linearizing the N-link system, with nonlinear equations of motion (1), about $(\Theta, \dot{\Theta}) \equiv 0$ yields

$$M \delta\ddot{\Theta} + C_d \delta\dot{\Theta} + K \delta\Theta = \Upsilon, \tag{2}$$

where

$$M \triangleq \begin{bmatrix} \gamma_{1,1} & \cdots & \gamma_{1,N} \\ \vdots & \ddots & \vdots \\ \gamma_{N,1} & \cdots & \gamma_{N,N} \end{bmatrix},$$

$$C_d \triangleq \begin{bmatrix} c_1 + c_2 & -c_2 & 0 & \ldots & 0 \\ -c_2 & c_2 + c_3 & -c_3 & \ldots & 0 \\ 0 & -c_3 & c_3 + c_4 & \ldots & 0 \\ \vdots & \vdots & \vdots & \ddots & \vdots \\ 0 & 0 & 0 & \ldots & c_N \end{bmatrix},$$

$$K \triangleq \begin{bmatrix} k_1 + k_2 & -k_2 & 0 & \ldots & 0 \\ -k_2 & k_2 + c_3 & -k_3 & \ldots & 0 \\ 0 & -k_3 & k_3 + k_4 & \ldots & 0 \\ \vdots & \vdots & \vdots & \ddots & \vdots \\ 0 & 0 & 0 & \ldots & k_N \end{bmatrix},$$

where, for $g = 1, ..., N$, and $h = g + 1, ..., N$, $\gamma_{g,g} \triangleq \left(\frac{m_g}{3} + \sum_{i=g+1}^{N} m_i \right) l_g^2$, and $\gamma_{g,h} \triangleq \left(\frac{m_h}{2} + \sum_{i=h+1}^{N} m_i \right) l_g l_h$, and, for $g, h = 1, ..., N$, $\gamma_{h,g} = \gamma_{g,h}$.

III. Retrospective Cost Model Reference Adaptive Control

In this section, we review the RC-MRAC algorithm presented in [18]. We highlight the model information required by the adaptive controller as well as several important assumptions. For additional details and a stability analysis of RC-MRAC, see [18].

First, consider the linear discrete-time system

$$y(k) = \sum_{i=1}^{n} -\alpha_i y(k-i) + \sum_{i=d}^{n} \beta_i u(k-i), \tag{3}$$

where $k \geq 0$, $\alpha_1, \ldots, \alpha_n \in \mathbb{R}$, $\beta_d, \ldots, \beta_n \in \mathbb{R}$, $y(k)$ is the output, $u(k)$ is the control, and the relative degree is $d > 0$.

Let $\mathbf{q}$ and $\mathbf{q}^{-1}$ denote the forward-shift and backward-shift operators, respectively, and define $\beta(\mathbf{q}) \triangleq \beta_d \mathbf{q}^{n-d} + \beta_{d+1} \mathbf{q}^{n-d-1} + \cdots + \beta_{n-1} \mathbf{q} + \beta_n$. Consider the factorization $\beta(\mathbf{q}) = \beta_d \beta_{\mathrm{u}}(\mathbf{q}) \beta_{\mathrm{s}}(\mathbf{q})$, where $\beta_{\mathrm{u}}(\mathbf{q})$ is a monic polynomial of degree n_u; $\beta_{\mathrm{s}}(\mathbf{q})$ is a monic polynomial; and if $\lambda \in \mathbb{C}$, $|\lambda| \geq 1$, and $\beta(\lambda) = 0$, then $\beta_{\mathrm{u}}(\lambda) = 0$ and $\beta_{\mathrm{s}}(\lambda) \neq 0$. We assume that the polynomial $\beta_{\mathrm{u}}(\mathbf{q})$ is known, which implies that the nonminimum-phase zeros from u to y are known. Furthermore, we assume that the first nonzero Markov parameter β_d is known.

Next, consider the reference model

$$\alpha_{\mathrm{m}}(\mathbf{q}) y_{\mathrm{m}}(k) = \beta_{\mathrm{m}}(\mathbf{q}) r(k), \tag{4}$$

where $y_{\mathrm{m}}(k) \in \mathbb{R}$ is the reference model output; $r(k) \in \mathbb{R}$ is the bounded reference model command; $\alpha_{\mathrm{m}}(\mathbf{q})$ is a monic polynomial with degree $n_{\mathrm{m}} > 0$; $\beta_{\mathrm{m}}(\mathbf{q})$ is a polynomial with degree $n_{\mathrm{m}} - d_{\mathrm{m}}$, where $d_{\mathrm{m}} \geq d$ is the relative degree of (4); and if $\lambda \in \mathbb{C}$, $|\lambda| \geq 1$, and $\beta_{\mathrm{u}}(\lambda) = 0$, then $\beta_{\mathrm{m}}(\lambda) = 0$.

Next, define $z(k) \triangleq y(k) - y_{\mathrm{m}}(k)$. Our goal is to drive $z(k)$ to zero. We use a time-series controller of order $n_{\mathrm{c}} \geq$

$\max(2n - n_{\rm u} - d, n_{\rm m} - n_{\rm u} - d)$, which is given by

$$u(k) = \sum_{i=1}^{n_{\rm c}} L_i(k)y(k-i) + \sum_{i=1}^{n_{\rm c}} M_i(k)u(k-i) + \sum_{i=0}^{n_{\rm c}} N_i(k)r(k-i), \quad (5)$$

where, for all $i = 1, \ldots, n_{\rm c}$, $L_i : \mathbb{N} \to \mathbb{R}$ and $M_i : \mathbb{N} \to \mathbb{R}$, and, for all $i = 0, 1, \ldots, n_{\rm c}$, $N_i : \mathbb{N} \to \mathbb{R}$ are determined by the adaptive law presented below. The controller (5) can be expressed as

$$u(k) = \phi^{\rm T}(k)\theta_{\rm c}(k), \quad (6)$$

where $\theta_{\rm c}(k) \triangleq [L_1(k) \ \cdots \ L_{n_{\rm c}}(k) \ M_1(k) \ \cdots \ M_{n_{\rm c}}(k) \ N_0(k) \ \cdots \ N_{n_{\rm c}}(k)]^{\rm T}$, and $\phi(k) \triangleq [\ y(k-1) \ \cdots \ y(k-n_{\rm c}) \ u(k-1) \ \cdots \ u(k-n_{\rm c}) \ r(k) \ \cdots \ r(k-n_{\rm c})]^{\rm T}$.

Now, let $\hat{\theta} \in \mathbb{R}^{3n_{\rm c}+1}$ be an optimization variable, and define the retrospective performance

$$\hat{z}_{\rm f}(\hat{\theta}, k) \triangleq z_{\rm f}(k) + \Phi^{\rm T}(k)\hat{\theta} - \beta_d\bar{\beta}_{\rm u}(\mathbf{q}^{-1})u(k),$$

where $\bar{\beta}_{\rm u}(\mathbf{q}^{-1}) \triangleq \mathbf{q}^{-n_{\rm u}-d}\beta_{\rm u}(\mathbf{q})$, the filtered tracking error is defined by $z_{\rm f}(k) \triangleq \mathbf{q}^{-n_{\rm m}}\alpha_{\rm m}(\mathbf{q})z(k)$, and the filtered regressor is defined by $\Phi(k) \triangleq \beta_d\bar{\beta}_{\rm u}(\mathbf{q}^{-1})\phi(k)$.

Finally, define the cumulative retrospective cost function

$$J(\hat{\theta}, k) \triangleq \sum_{i=0}^{k} \lambda^{k-i}\hat{z}_{\rm f}^2(\hat{\theta}, i) + \lambda^k \left[\hat{\theta} - \theta(0)\right]^{\rm T} R \left[\hat{\theta} - \theta(0)\right],$$

where $\lambda \in (0, 1]$, $R \in \mathbb{R}^{(3n_{\rm c}+1)\times(3n_{\rm c}+1)}$ is positive definite, and $\theta(0) \in \mathbb{R}^{3n_{\rm c}+1}$. For each $k \geq 0$, $J(\hat{\theta}, k)$ is minimized by the recursive-least-squares algorithm with a forgetting factor

$$\theta_{\rm c}(k+1) = \theta_{\rm c}(k) - \frac{P(k)\Phi(k)z_{\rm f,r}(k)}{\lambda + \Phi^{\rm T}(k)P(k)\Phi(k)}, \quad (7)$$

$$P(k+1) = \frac{1}{\lambda}\left[P(k) - \frac{P(k)\Phi(k)\Phi^{\rm T}(k)P(k)}{\lambda + \Phi^{\rm T}(k)P(k)\Phi(k)}\right], \quad (8)$$

where $P(0) = R^{-1}$ and $z_{\rm f,r}(k) \triangleq \hat{z}_{\rm f}(\theta_{\rm c}(k), k)$. In summary, RC-MRAC is given by (6)–(8), and its architecture is shown in Figure 2.

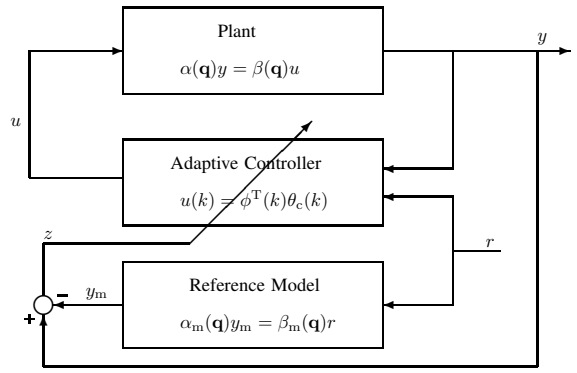

Fig. 2. Schematic diagram of RC-MRAC given by (6), (7), and (8).

IV. Implementation of RC-MRAC

In this section, we discuss implementation of RC-MRAC on the N-link planar arm. We implement RC-MRAC with a zero-order hold on the inputs and a sampling time $T_{\rm s} = 0.02$ seconds. Although the RC-MRAC formulation, presented in Section III, is based on a linear plant, we apply RC-MRAC to the full nonlinear N-link planar arm, given by (1).

We assume that the control torque at the hub of the N-link planar arm (i.e., v_1) is the only available control input. Thus, $v_2, \ldots, v_N$ in (1) are identically zero and v_1 is the zero order hold of $u(k)$, where $u(k)$ is determined by RC-MRAC (6)–(8). We assume that the angular position of the $N^{\rm th}$ link (i.e., θ_N) is the only measurement available for feedback. Thus, $y(k)$ is the sampled-data signal obtained from θ_N. Our objective is to force the angular position of the $N^{\rm th}$ link to follow the reference model output $y_{\rm m}(k)$.

In order to implement RC-MRAC, we require knowledge of $\beta_{\rm u}(\mathbf{q})$, which characterizes the nonminimum-phase zeros of the linearized N-link system from the control torque at the hub to the angular position of the $N^{\rm th}$ link. It is shown in [6] that the linearized transfer function of the 2-link system from v_1 to $\delta\theta_2$ has exactly one nonminimum-phase zero. Furthermore, [6] provides numerical evidence that the linearized transfer function of the N-link system from v_1 to $\delta\theta_N$ (i.e., from the hub to the tip of the multilink mechanism) has $N-1$ nonminimum-phase zeros. Finally, discretizing the linearized transfer function from v_1 to $\delta\theta_N$ (using a zero-order hold on the inputs) results in a discrete-time transfer function, which in general also has $N-1$ nonminimum-phase zeros. The locations of the nonmimum-phase zeros depend on the sampling time used for the discretization. In this numerical study, we let $\beta_{\rm u}(\mathbf{q})$ be the polynomial whose roots are at the nonminimum-phase zero locations obtained from the discretized linearization.

V. Simulation Results

In this section, we use RC-MRAC to control the nonlinear N-link system. In particular, for the two, three, and four link cases, we numerically investigate the performance of RC-MRAC with sinusoidal reference model commands $r(k)$. Our goal is to explore the amplitude and frequency ranges of the reference model output $y_{\rm m}(k)$ for which the output of the N-link system $y(k)$ is able to track $y_{\rm m}(k)$. We demonstrate that RC-MRAC is able to control the N-link system for a range of reference model output amplitudes and frequencies; however, for large-amplitude or high-frequency reference model outputs the N-link system's nonlinearities become difficult for RC-MRAC to control.

For all examples, the controller order is $n_{\rm c} = 12$ and the reference model is given by (4). Next, define the reference model transfer function $G_{\rm m}(\mathbf{z}) \triangleq \frac{\beta_{\rm m}(\mathbf{z})}{\alpha_{\rm m}(\mathbf{z})}$ and consider the reference model command

$$r(k) = \frac{A}{|G_{\rm m}(e^{\jmath\omega T_{\rm s}})|}\sin\omega T_{\rm s}k,$$

where ω is the frequency in rad/sec and A is the amplitude in rad. Note that the amplitude of $r(k)$ is normalized by the

magnitude of the reference model transfer function at the command frequency (i.e., $|G_{\rm m}(e^{\jmath\omega T_{\rm s}})|$). The normalization is performed so that, for any frequency ω, the steady-state amplitude of $y_{\rm m}(k)$ is A. Thus, we can independently vary the amplitude A and frequency ω of the steady-state reference model output $y_{\rm m}(k)$, which is the signal that the adaptive controller is attempting to track. Finally, for all examples, $\theta_{\rm c}(0) = 0$ and $\lambda = 1$.

A. The Two-Link Case

We consider the 2-link system, where $m_1 = 2$ kg, $m_2 = 3$ kg, $l_1 = 2$ m, $l_2 = 1$ m, $k_1 = 7\ \frac{\rm N-m}{\rm rad}$, $k_2 = 5\ \frac{\rm N-m}{\rm rad}$, $c_1 = 10\ \frac{\rm kg-m^2}{\rm rad}$, and $c_2 = 10\ \frac{\rm kg-m^2}{\rm rad}$. In this case, $\beta_d = -8.045\times10^{-5}$ and $\beta_{\rm u}(\mathbf{q}) = \mathbf{q} - 1.0784$. Additionally, we let $\alpha_{\rm m}(\mathbf{q}) = (\mathbf{q}-0.8)^5$, $\beta_{\rm m}(\mathbf{q}) = \mathbf{q}\beta_{\rm u}(\mathbf{q})$, and $P(0) = 10^{12}I_{37}$.

The 2-link system is simulated for a range of reference model output amplitudes and frequencies; specifically, A is varied from 0 rad to 1 rad, and ω is varied from 0 rad/sec to 20π rad/sec. For each choice of A and ω, the 2-link system is simulated for 20 seconds, and we explore the values of A and ω for which RC-MRAC drives the performance $z(k)$ to zero. If the angular position of the second link exceeds 2π rad, then we consider this transient behavior to exceed acceptable limits, meaning that RC-MRAC is not effective. Next, for each simulation, define the performance metric

$$\varepsilon = \max_{0\le k\le \frac{20}{T_{\rm s}}} |z(k)|\,, \tag{9}$$

which quantifies the peak transient tracking error.

Figure 3 is a heat map, which shows the range of reference model output amplitudes A and reference model command frequencies ω, where RC-MRAC is effective. Furthermore, the color at each point on the heat map indicates the value of ε. Finally, the white regions correspond to the values of A and ω where the angular position of the second link exceeds 2π rad. Figure 3 demonstrates that RC-MRAC is effective over a large amplitude range when the frequency is low, and over a large frequency range when the amplitude is small.

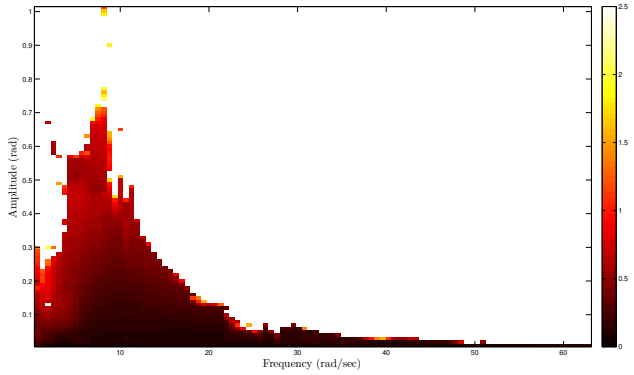

Fig. 3. *Two-Link System Heat Map:* The heat map for the two-link system shows that RC-MRAC effectively controls the 2-link system over a range of reference model output amplitudes and frequencies. White regions represent a response greater than 2π radians.

Next, we explore two values of A and ω in more detail. In particular, we consider an (A, ω) pair, which is in the colored region of the heat map but not near the boundary; and an (A, ω) pair, which is in the colored region of the heat map and near the boundary.

Example 1. Let $A = 0.3$ and $\omega = 2\pi$, which is in the colored region of the heat map but not near the boundary. Figure 4 shows the closed-loop response of the 2-link system with RC-MRAC in feedback. The 2-link system is allowed to run open loop for 5 seconds, then RC-MRAC is turned on. The top plot of Figure 4 shows that $y(k)$ asymptotically follows $y_{\rm m}(k)$. The middle and bottom plots of Figure 4 provide a time history of the angles θ_1 and θ_2, and the rates $\dot\theta_1$ and $\dot\theta_2$.

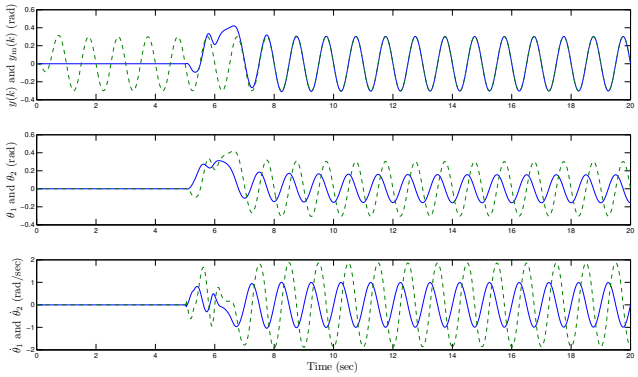

Fig. 4. *Example 1:* For the 2-link system with $A = 0.3$ and $\omega = 2\pi$, the angular position of the second link $y(k)$ follows the reference model output $y_{\rm m}(k)$. Top plot shows $y(k)$ (solid) and $y_{\rm m}(k)$ (dashed); middle plot shows the angles θ_1 (solid) and θ_2 (dashed); bottom plot shows the angular rates $\dot\theta_1$ (solid) and $\dot\theta_2$ (dashed).

Example 2. Let $A = 0.01$ and $\omega = 10\pi$, which is in the colored region of the heat map and near the boundary. Figure 5 shows the closed-loop response of the 2-link system with RC-MRAC in feedback. The top plot of Figure 5 shows that $y(k)$ asymptotically follows $y_{\rm m}(k)$; however, the transient performance is worse than that shown in Figure 5. Note that the plots have been truncated after 10 seconds.

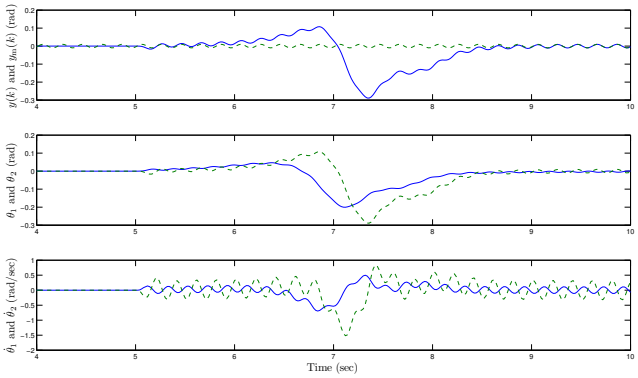

Fig. 5. *Example 2:* For the 2-link system with $A = 0.01$ and $\omega = 10\pi$, the angular position of the second link $y(k)$ follows the reference model output $y_{\rm m}(k)$. However, the transient behavior for this example is worse than the transient behavior shown in Figure 4. Top plot shows $y(k)$ (solid) and $y_{\rm m}(k)$ (dashed); middle plot shows the angles θ_1 (solid) and θ_2 (dashed); bottom plot shows the angular rates $\dot\theta_1$ (solid) and $\dot\theta_2$ (dashed).

B. The Three-Link Case

We consider the 3-link system, where $m_1 = 2$ kg, $m_2 = 3$ kg, $m_3 = 4$ kg, $l_1 = 2$ m, $l_2 = 1$ m, $l_3 = 1$ m, $k_1 = 7$ $\frac{\text{N-m}}{\text{rad}}$, $k_2 = 5$ $\frac{\text{N-m}}{\text{rad}}$, $k_3 = 6$ $\frac{\text{N-m}}{\text{rad}}$, $c_1 = 10$ $\frac{\text{kg-m}^2}{\text{rad}}$, $c_2 = 10$ $\frac{\text{kg-m}^2}{\text{rad}}$, and $c_3 = 1$ $\frac{\text{kg-m}^2}{\text{rad}}$. In this case, $\beta_d = 2.13 \times 10^{-6}$ and $\beta_{\text{u}}(\mathbf{q}) = (\mathbf{q} - 1.016)(\mathbf{q} - 18.90)$. Additionally, we let $\alpha_{\text{m}}(\mathbf{q}) = (\mathbf{q} - 0.9)^5$, $\beta_{\text{m}}(\mathbf{q}) = \beta_{\text{u}}(\mathbf{q})$, and $P(0) = 10^{17} I_{37}$.

The 3-link system is simulated for a range of reference model output amplitudes and frequencies; specifically, A is varied from 0 rad to 0.5 rad, and ω is varied from 0 rad/sec to 10π rad/sec. We use the performance metric ε given by (9) and consider transient behavior to exceed acceptable limits if the angular position of the third link exceeds 2π rad. Figure 6 is the heat map for the 3-link system. Notice that the shape of Figure 6 is similar to the shape of Figure 3 (i.e., the heat map for the 2-link system). However, RC-MRAC is effective over a smaller range of values of A and ω in the 3-link case. The smaller range of (A, ω) may be a result of the additional nonlinearities that arise when additional links are added to the multilink arm.

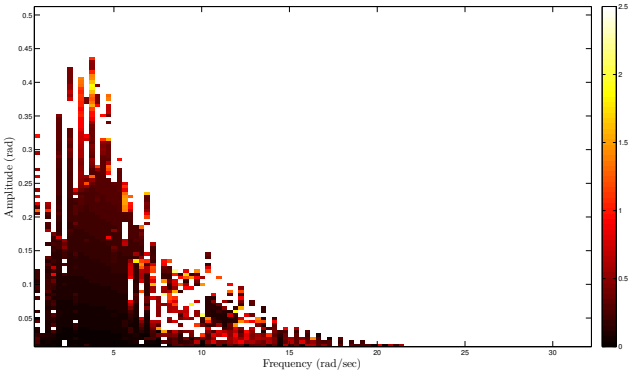

Fig. 6. *Three-Link System Heat Map:* The heat map for the three-link system shows that RC-MRAC effectively controls the 3-link system over a range of reference model output amplitudes and frequencies. White regions represent a response greater than 2π radians.

Example 3. Let $A = 0.1$ and $\omega = \pi$, which is in the colored region of the heat map but not near the boundary. Figure 7 shows the closed-loop response of the 3-link system with RC-MRAC in feedback. The 3-link system is allowed to run open loop for 5 seconds, then RC-MRAC is turned on. The top plot of Figure 7 shows that $y(k)$ asymptotically follows $y_{\text{m}}(k)$.

Example 4. Let $A = 0.01$ and $\omega = 5\pi$, which is in the colored region of the heat map and near the boundary. Figure 8 shows the closed-loop response of the 3-link system with RC-MRAC in feedback. The top plot of Figure 8 shows that $y(k)$ asymptotically follows $y_{\text{m}}(k)$; however, the transient performance is worse than that shown in Figure 7.

C. The Four-Link Case

We consider the 4-link system, where $m_1 = 2$ kg, $m_2 = 3$ kg, $m_3 = 4$ kg, $m_4 = 3$ kg, $l_1 = 2$ m, $l_2 = 1$ m, $l_3 = 1$ m, $l_4 = 1$ m, $k_1 = 7$ $\frac{\text{N-m}}{\text{rad}}$, $k_2 = 5$ $\frac{\text{N-m}}{\text{rad}}$, $k_3 = 6$ $\frac{\text{N-m}}{\text{rad}}$, $k_4 = 5$

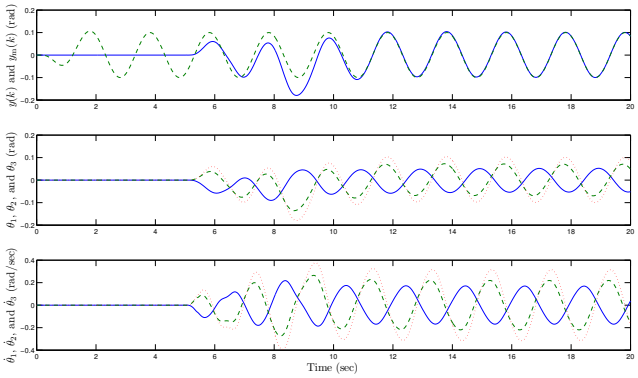

Fig. 7. *Example 3:* For the 3-link system with $A = 0.1$ and $\omega = \pi$, the angular position of the third link $y(k)$ follows the reference model output $y_{\text{m}}(k)$. Top plot shows $y(k)$ (solid) and $y_{\text{m}}(k)$ (dashed); middle plot shows the angles θ_1 (solid), θ_2 (dashed), and θ_3 (dotted); bottom plot shows the angular rates $\dot{\theta}_1$ (solid), $\dot{\theta}_2$ (dashed), and $\dot{\theta}_3$ (dotted).

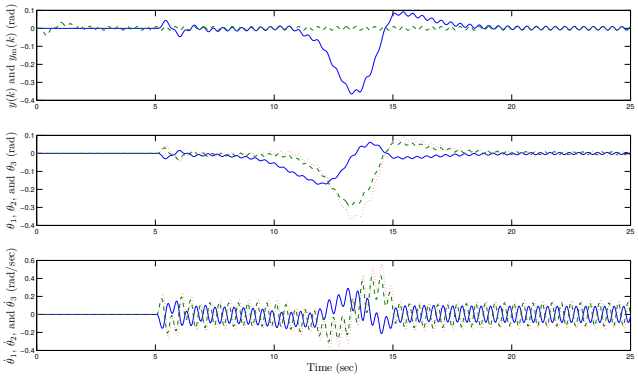

Fig. 8. *Example 4:* For the 3-link system with $A = 0.01$ and $\omega = 5\pi$, the angular position of the third link $y(k)$ follows the reference model output $y_{\text{m}}(k)$. However, the transient behavior for this example is worse than the transient behavior shown in Figure 7. Top plot shows $y(k)$ (solid) and $y_{\text{m}}(k)$ (dashed); middle plot shows the angles θ_1 (solid), θ_2 (dashed), and θ_3 (dotted); bottom plot shows the angular rates $\dot{\theta}_1$ (solid), $\dot{\theta}_2$ (dashed), and $\dot{\theta}_3$ (dotted).

$\frac{\text{N-m}}{\text{rad}}$, $c_1 = 10$ $\frac{\text{kg-m}^2}{\text{rad}}$, $c_2 = 10$ $\frac{\text{kg-m}^2}{\text{rad}}$, $c_3 = 1$ $\frac{\text{kg-m}^2}{\text{rad}}$, and $c_4 = 9$ $\frac{\text{kg-m}^2}{\text{rad}}$. In this case, $\beta_d = 2.44 \times 10^{-6}$ and $\beta_{\text{u}}(\mathbf{q}) = (\mathbf{q} - 1.008)(\mathbf{q} - 1.649)(\mathbf{q} + 4.684)$. Additionally, we let $\alpha_{\text{m}}(\mathbf{q}) = (\mathbf{q} - 0.9)^5$, $\beta_{\text{m}}(\mathbf{q}) = \beta_{\text{u}}(\mathbf{q})$, and $P(0) = 10^{19} I_{37}$.

The 4-link system is simulated for A from 0 rad to 0.15 rad, and ω is varied from 0 rad/sec to 6π rad/sec. We use the performance metric ε given by (9). Figure 9 is the heat map for the 4-link system. The shape of Figure 9 is similar to the shapes of Figure 3 and Figure 6, but the range of (A, ω) where RC-MRAC is effective is smaller than in the 3-link case (which is smaller than in the 2-link case). This provides additional numerical evidence that the range of achievable motion (i.e., the amplitude and frequency of the reference model output) decreases as the number of links increases.

Example 5. Let $A = 0.02$ and $\omega = 2\pi$, which is in the colored region of the heat map but not near the boundary. Figure 10 shows the closed-loop response of the 4-link system with RC-MRAC in feedback. The top plot of Figure 10 shows that $y(k)$ asymptotically follows $y_{\text{m}}(k)$.

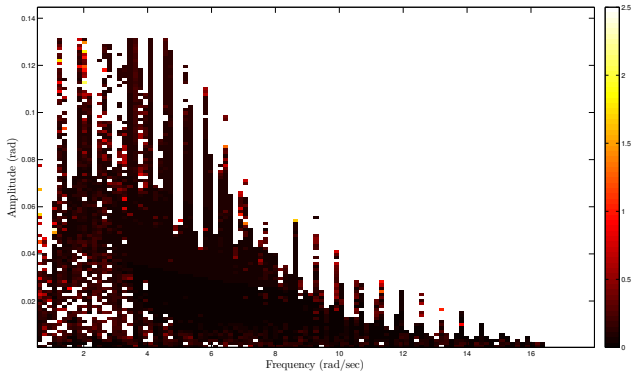

Fig. 9. *Four-Link System Heat Map:* The heat map for the four-link system shows that RC-MRAC effectively controls the 4-link system over a range of reference model output amplitudes and frequencies. White regions represent a response greater than 2π radians.

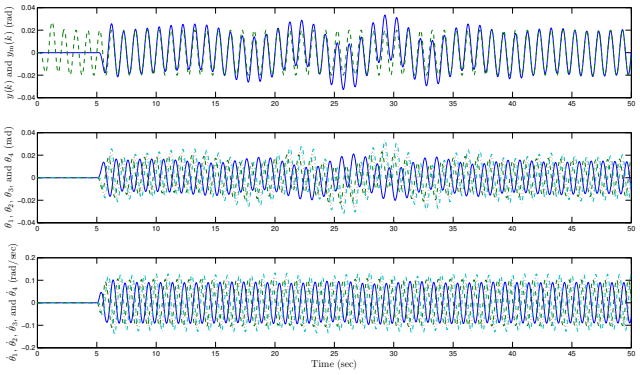

Fig. 10. *Example 5:* For the 4-link system with $A = 0.02$ and $\omega = 2\pi$, the angular position of the fourth link $y(k)$ follows the reference model output $y_{\rm m}(k)$. Top plot shows $y(k)$ (solid) and $y_{\rm m}(k)$ (dashed); middle plot shows the angles θ_1 (solid), θ_2 (dashed), θ_3 (dotted), and θ_4 (dash-dotted); bottom plot shows the angular rates $\dot{\theta}_1$ (solid), $\dot{\theta}_2$ (dashed), $\dot{\theta}_3$ (dotted), and $\dot{\theta}_4$ (dash-dotted).

Example 6. Let $A = 0.001$ and $\omega = 5\pi$, which is in the colored region of the heat map and near the boundary. Figure 11 shows the closed-loop response of the 4-link system with RC-MRAC in feedback. The top plot of Figure 11 shows that $y(k)$ asymptotically follows $y_{\rm m}(k)$; however, the transient performance is worse than that shown in Figure 10.

VI. Conclusion

This paper addressed the model reference adaptive control problem for a nonlinear N-link planar arm mechanism, where the linearized transfer function from the control torque applied at the hub to the angular position of the $N^{\rm th}$ link is nonminimum-phase. We used the RC-MRAC algorithm to effectively control the multilink arm for a range of reference model output signal amplitudes and frequencies. We demonstrated that, for the 2-link, 3-link, and 4-link cases, RC-MRAC is effective for controlling the multilink arm. However, the range of admissible reference model output amplitudes and frequencies decreases as the number of links increases.

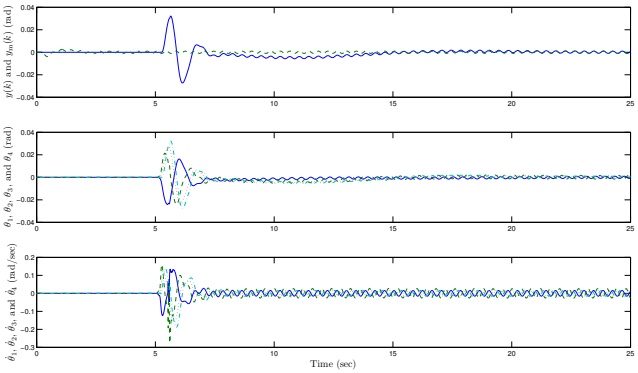

Fig. 11. *Example 6:* For the 4-link system with $A = 0.001$ and $\omega = 5\pi$, the angular position of the fourth link $y(k)$ follows the reference model output $y_{\rm m}(k)$. However, the transient behavior for this example is worse than the transient behavior shown in Figure 10. Top plot shows $y(k)$ (solid) and $y_{\rm m}(k)$ (dashed); middle plot shows the angles θ_1 (solid), θ_2 (dashed), θ_3 (dotted), and θ_4 (dash-dotted); bottom plot shows the angular rates $\dot{\theta}_1$ (solid), $\dot{\theta}_2$ (dashed), $\dot{\theta}_3$ (dotted), and $\dot{\theta}_4$ (dash-dotted).

References

[1] M. J. Balas, "Direct velocity feedback control of large space structures," *AIAA J. Guid. Contr. Dyn.*, vol. 2, no. 3, pp. 252–253, 1979.

[2] R. H. Cannon and D. E. Rosenthal, "Experiments in control of flexible structures with noncolocated sensors and actuators," *AIAA J. Guid. Contr. Dyn.*, vol. 7, no. 5, pp. 546–553, 1984.

[3] D. Abramovitch and G. Franklin, "A brief history of disk drive control," *IEEE Contr. Sys. Mag.*, vol. 22, no. 3, pp. 28–42, 2002.

[4] B. P. Rigney, L. Y. Pao, and D. A. Lawrence, "Nonminimum phase dynamic inversion for settle time applications," *IEEE Trans. Contr. Sys. Tech.*, vol. 17, pp. 989–1005, 2009.

[5] D. K. Miu, *Mechatronics*. New York: Springer-Verlag, 1993.

[6] A. V. Morozov, J. B. Hoagg, and D. S. Bernstein, "Retrospective cost adaptive control of a planar multilink arm with nonminimum-phase zeros," in *Proc. Conf. Dec. Contr.*, Atlanta, GA, December 2010, pp. 3706–3711.

[7] J. C. Doyle, B. A. Francis, and A. R. Tannenbaum, *Feedback Control Theory*. New York: Macmillan, 1992.

[8] M. Vidyasagar, "On undershoot and nonminimum phase zeros," *IEEE Trans. Autom. Contr.*, vol. 31, p. 440, 1986.

[9] J. B. Hoagg and D. S. Bernstein, "Nonminimum-phase zeros: Much to do about nothing," *IEEE Contr. Sys. Mag.*, vol. 27, pp. 45–57, June 2007.

[10] J. Hong and D. S. Bernstein, "Bode integral constraints, colocation, and spillover in active noise and vibration control," *IEEE Trans. Contr. Sys. Tech.*, vol. 6, pp. 111–120, 1998.

[11] J. B. Hoagg, J. Chandrasekar, and D. S. Bernstein, "On the zeros, initial undershoot, and relative degree of lumped-mass structures," *ASME J. Dynamical Systems, Measurement, and Contr.*, vol. 129, pp. 493–502, 2007.

[12] J. L. Lin, "On transmission zeros of mass-dashpot-spring systems," *J. Dynamical Systems, Measurement, and Contr.*, vol. 121, pp. 179–183, 1999.

[13] D. K. Miu, "Physical interpretation of transfer function zeros for simple control systems with mechanical flexibilities," *J. Dynamical Systems, Measurement, and Contr.*, vol. 113, pp. 419–424, 1991.

[14] E. H. Maslen, "Positive real zeros in flexible beams," *Shock and Vibration*, vol. 2, pp. 429–435, 1995.

[15] M. A. Santillo and D. S. Bernstein, "Adaptive control based on retrospective cost optimization," *AIAA J. Guid. Contr. Dyn.*, vol. 33, pp. 289–304, 2010.

[16] J. B. Hoagg and D. S. Bernstein, "Cumulative retrospective cost adaptive control with RLS-based optimization," in *Proc. Amer. Contr. Conf.*, Baltimore, MD, June 2010, pp. 4016–4021.

[17] ——, "Retrospective cost adaptive control for nonminimum-phase discrete-time systems, Part 1 and Part 2," in *Proc. Conf. Dec. Contr.*, Atlanta, GA, December 2010, pp. 893–904.

[18] ——, "Retrospective cost model reference adaptive control for nonminimum-phase discrete-time systems, Part 1 and Part 2," in *Proc. Amer. Contr. Conf.*, San Francisco, CA, June 2011, pp. 2927–2938.